Adaptive fixed-time trajectory tracking control of a stratospheric airship

Zheng, Zewei; Feroskhan, Mir; Sun, Liang

2018

Zheng, Z., Feroskhan, M., & Sun, L. (2018). Adaptive fixed-time trajectory tracking control of a stratospheric airship. ISA Transactions, 76, 134-144. doi:10.1016/j.isatra.2018.03.016

https://hdl.handle.net/10356/105451

https://doi.org/10.1016/j.isatra.2018.03.016

Adaptive fixed-time trajectory tracking control of a stratospheric airship

Zewei Zheng, Mir Feroskhan, Liang Sun

Abstract

This paper addresses the fixed-time trajectory tracking control problem of a stratospheric airship. By extending the method of adding a power integrator to a novel adaptive fixed-time control method, the convergence of a stratospheric airship to its reference trajectory is guaranteed to be achieved within a fixed time. The control algorithm is firstly formulated without the consideration of external disturbances to establish the stability of the closed-loop system in fixed-time and demonstrate that the convergence time of the airship is essentially independent of its initial conditions. Subsequently, a smooth adaptive law is incorporated into the proposed fixed-time control framework to provide the system with robustness to external disturbances. Theoretical analyses demonstrate that under the adaptive fixed-time controller, the tracking errors will converge towards a residual set in fixed-time. The results of a comparative simulation study with other recent methods illustrate the remarkable performance and superiority of the proposed control method.

Keywords: adaptive control, fixed-time control, stratospheric airship, trajectory tracking

1. Introduction

The stratosphere has promptly garnered special attention from the aviation research industry that aims to capitalize on its stable meteorological conditions. This serves as motivation to develop long endurance stratospheric aircrafts that possess the capacity to play a significant role in surveillance and intelligence, earth observation, telecommunications and environmental monitoring, similar to satellites. As such, the design of the stratospheric aircraft takes the form of lighter-than-air aerostats such as balloons[1] and airships[2–5], unlike the conventional aeroplane, as aerostats generally rely on buoyancy rather than aerodynamic lift for flight. The stratospheric airship is more advantageous operationally than satellites because it can be launched at a much lower cost, is reusable and can be conveniently maintained. Unlike the balloon, the stratospheric airship is also able to fly precisely along a scheduled route, also known as trajectory tracking, to cater to a wider range of mission objectives [6–10]. However, the tracking control design poses challenges since the airship is an inherently nonlinear and highly coupled multi-input multi-output (MIMO) system with unknown external disturbances.

There are several control methods for the trajectory tracking of the stratospheric airship that have been covered in the following literature. Based on an active disturbance rejection method to handle the external disturbances, a robust nonlinear controller was proposed for the trajectory tracking of an airship [11]. However, the controller was developed based on a simplified airship dynamic model where the airship's motion is limited to yawing and translation along the horizontal plane. The authors in [12] utilized a non-certainty equivalence adaptive approach to develop a trajectory tracking controller that accommodates the uncertain mass and inertia parameters of a fully-actuated stratospheric airship. Together with neural network approximation, another control approach that involves a terminal sliding mode surface is adopted for a robotic airship in [13]. The case of an under-actuated airship control problem was studied in [14], where an integrator backstepping controller based on the Lyapunov theory was shown to provide stability in its ascent and descent maneuvers. In [15], a rigorous multi-loop control structure for the trajectory tracking of the airship was formulated based on trajectory linearization control technique. A path tracking gain-scheduling controller that caters to controlling both the lateral and longitudinal motions simultaneously, was designed in [16] for an airship subjected to wind disturbances. In addition to the trajectory tracking control, many other control schemes were also widely researched for airships, such as attitude control [17], hovering control [18], path following control [19–21], and specific configuration airship control [22, 23].

The aforementioned control approaches can only guarantee asymptotical convergence, which means that the setting time is infinite. However, in the airship design, the convergence time is an important design index that needs to be set explicitly. Alternatively, the finite-time control schemes[3, 24–26] can provide a faster convergence rate and the system states will reach equilibrium within a finite time. However, the setting time for the finite-time methods depends on the initial states of the system. This prohibits the application of finite-time methods in the scenario where information on the initial states are unavailable or inaccurate. In contrast, the fixed-time stability concept [27] was proposed to acquire a fixed maximum settling time that can be estimated and is independent of the initial states. Moreover, it performs uniformly for the fixed-time control under different initial conditions and its control parameters are not required to be re-tuned to sustain the convergence time [28–30].

Research in fixed-time control methods is rather recent and not yet exhaustive. In [29, 30], by extending the method of adding a power integrator, the fixed-time control solutions for nonlinear systems and Euler-Lagrange systems are presented.

However, these methods are theoretical results and cannot be applied directly to actual aircraft objects. In [31], a fixed-time non-recursive differentiator algorithm was implemented in a hypersonic missile simulation. Based on the nonsingular terminal sliding mode protocol developed by [32], a leader-following fixed-time consensus controller was successfully employed for multi-agent systems that contain input delay [33]. On the other hand, for the multi-agent systems in the presence of external disturbance, a cascade structure [34] that integrate a fixed-time consensus protocol with a fixed-time observer [35] was presented to ensure the fixed-time consensus tracking. In [36, 37], fixed-time fault-tolerant controllers that incorporated a sliding mode surface were developed for the spacecraft that is being subjected to thruster faults and actuator saturation. Although several literature regarding the fixed-time control for different systems have been documented, the fixed-time tracking design for nonlinear systems in the presence of unknown external disturbances is still an open issue.

Motivated by the aforementioned analyses and inspired by [29, 30], this paper presents an adaptive fixed-time trajectory tracking control scheme for a stratospheric airship under external disturbances. The main contributions and the key features of the proposed method are summarized as follows.

1) A new globally fixed-time tracking control method is designed using the method of adding a power integrator. If the disturbances are not considered, the method ensures that the tracking errors converge to zero within a fixed time.
2) An adaptive algorithm that estimates the bound of unknown disturbances is incorporated into the proposed controller to alleviate the effects of disturbances that results in better system robustness. The tracking errors will converge towards a residual set in fixed-time.
3) Unlike the fixed-time methods in [31–37], the control signals of the proposed method that lead to the fixed-time convergence of the tracking errors are smooth and the method does not contain any signum operator.

This paper is organized as follows. The preliminaries and the problem formulation are described in Section 2. Section 3 is devoted to formulating the fixed-time controllers for the stratospheric airship with external disturbances. Results of simulation are shown in Section 4. Section 5 concludes the paper.

2. Preliminaries and problem formulation

2.1. Preliminaries

Throughout this paper, $|\cdot|$ represents the absolute value of a scalar while $\|\cdot\|$ represents the Euclidean norm of a vector. For $\boldsymbol{a} \in \mathbb{R}^n$, $a_i, i = 1, 2, \cdots, n$ represents the ith component of $\boldsymbol{a}$, $\boldsymbol{a}^k = [a_1^k, a_2^k, \cdots, a_n^k]^T$, and $\lceil \boldsymbol{a}^k \rfloor = \text{diag}\{a_1^k, a_2^k, \cdots, a_n^k\}$. Consider the system

$$\dot{\boldsymbol{x}}(t) = \boldsymbol{f}(\boldsymbol{x}(t)),\ \boldsymbol{f}(\boldsymbol{0}) = \boldsymbol{0},\ \boldsymbol{x} \in \mathbb{R}^n \tag{1}$$

where $\boldsymbol{f} : D_0 \to \mathbb{R}^n$ is continuous on an open neighborhood D_0 of the origin. The definitions and lemmas that are required for the control design are delineated as follows.

Definition 1. [27] The equilibrium $\boldsymbol{x} = \boldsymbol{0}$ of (1) is fixed-time stable if it is globally finite-time stable and the settling-time function $T(\boldsymbol{x})$ is bounded, i.e. there is an existing positive constant T_{max} such that $T(\boldsymbol{x}) \leq T_{max}$ for any $\boldsymbol{x} \in \mathbb{R}^n$.

Lemma 1. [27] Suppose there is a Lyapunov function $V(\boldsymbol{x})$ defined on a neighborhood D of the origin and $\dot{V}(\boldsymbol{x}) \leq -(\alpha V(\boldsymbol{x})^p + \beta V(\boldsymbol{x})^g)^k$, where $\{\alpha, \beta, p, g, k\} \in \mathbb{R}^+$, $pk < 1$ and $gk > 1$, then the origin of (1) is fixed-time stable. As such, $V(\boldsymbol{x})$ from any initial position within the region D is able to converge to $V(\boldsymbol{x}) \equiv 0$ within a fixed time where the setting time T is bounded by $T \leq \frac{1}{\alpha^k(1-pk)} + \frac{1}{\beta(gk-1)}$.

Lemma 2. [36] Suppose the Lyapunov function $V(\boldsymbol{x})$ in Lemma 1 satisfies $\dot{V}(\boldsymbol{x}) \leq -(\alpha V(\boldsymbol{x})^p + \beta V(\boldsymbol{x})^g)^k + \vartheta$, where $\vartheta > 0$, then the origin of (1) is practical fixed-time stable, and the residual set is given by

$$\left\{\lim_{t\to T}\boldsymbol{x} | V(\boldsymbol{x}) \leq \min\left\{\alpha^{-\frac{1}{p}}\left(\frac{\vartheta}{1-\theta^k}\right)^{\frac{1}{kp}}, \beta^{-\frac{1}{p}}\left(\frac{\vartheta}{1-\theta^k}\right)^{\frac{1}{kg}}\right\}\right\}$$

where $\theta \in (0, 1]$. The setting time T required to attain the residual set is bounded by $T \leq \frac{1}{\alpha^k\theta^k(1-pk)} + \frac{1}{\beta\theta^k(gk-1)}$.

Lemma 3. [38] The inequality $0 \leq |x| - x\tanh(x/\eta) \leq \kappa\eta$ holds for any $\eta \in \mathbb{R}^+$ where $x \in \mathbb{R}$ and $\kappa = \mathrm{e}^{-(\kappa+1)}$.

Definition 2. Matrix $\text{Tanh}(\boldsymbol{x}) : \mathbb{R}^n \to \mathbb{R}^{n\times n}$ is defined as $\text{Tanh}(\boldsymbol{x}) = \text{diag}\{\tanh(x_1), \tanh(x_2), \cdots, \tanh(x_n)\}$.

Lemma 4. [24] For $\{m, n\} > 0$ and a positive function $a(x, y)$, there exists a positive function $c(x, y)$ such that $|a(x, y)x^m y^n| \leq c(x, y)|x|^{m+n} + \frac{n}{m+n}\left(\frac{m}{(m+n)c(x,y)}\right)^{\frac{m}{n}}|a(x, y)|^{\frac{m+n}{n}}|y|^{m+n}$.

Lemma 5. [30, 32] Let x_i, $i = 1, 2, \cdots, n$ be real numbers. In the case where $p > 0$, $(|x_1| + |x_2| + \cdots + |x_n|)^p \leq \max(n^{p-1}, 1)(|x_1|^p + |x_2|^p + \cdots + |x_n|^p)$. If $p = m/n \leq 1$, in which $\{m, n\} > 0$ are odd integers, $|x_1^p - x_2^p| \leq 2^{1-p}|x_1 - x_2|^p$.

2.2. Model of airship

Fig. 1 shows the stratospheric airship with a typical ellipsoidal ballonet. The ballonet that comprises of the helium gas generates the buoyancy force for lift. A gondola that is situated under the ballonet provides space for mounting the flight control, power and payload systems. The elevator and rudder that are located on the empennage of the airship provide the aerodynamic control deflections for yawing and pitching motions respectively. A propeller with vectored thrust capability is mounted on each side of the gondola to generate the thrust input for flight.

To develop the necessary dynamic models for the airship, the earth and body-fixed reference frames are firstly defined. The earth reference frame (ERF) is attached to a fixed point O_g on the ground of the earth, where the $O_g x_g$-axis points north, $O_g y_g$-axis points east, and the $O_g z_g$-axis points to the center of the earth. As shown in Fig. 1, instead of the center of gravity (CG), the body-fixed reference frame (BRF) is attached to the center of volume (CV) O of the airship, where the Ox-axis points

towards the front of the airship, Oz-axis points vertically downwards and Oy-axis points towards the direction perpendicular to both Ox-axis and Oz-axis. The direction of the Oy-axis points towards the starboard side of the airship as obtained by using the right-hand rule.

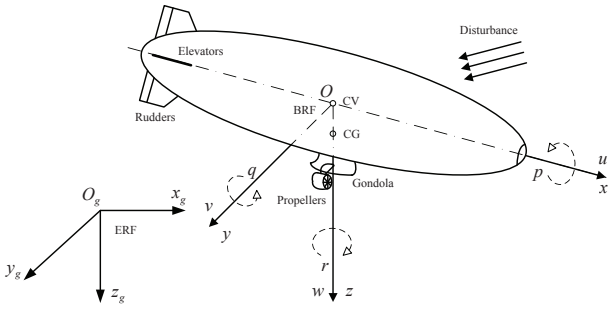

Figure 1: The schematic diagram of the stratospheric airship.

The position and attitude of the airship are $\boldsymbol{\zeta} = [x, y, z]^{\mathrm{T}}$ and $\boldsymbol{\gamma} = [\phi, \theta, \psi]^{\mathrm{T}}$ which are described with respect to ERF, where the ZYX Euler angle convention is adopted. The airship's velocity and angular velocity are $\boldsymbol{\upsilon} = [u, v, w]^{\mathrm{T}}$ and $\boldsymbol{\omega} = [p, q, r]^{\mathrm{T}}$ respectively, defined with respect to BRF. Consequently, the six degrees-of-freedom dynamic model for the stratospheric airship can be formulated as [12]

$$\begin{cases} \dot{\boldsymbol{x}} = \boldsymbol{R}\boldsymbol{y} \\ \boldsymbol{M}\dot{\boldsymbol{y}} = \boldsymbol{N}_1 + \boldsymbol{N}_2^* + \boldsymbol{N}_3 + \boldsymbol{B}\boldsymbol{\tau} + \boldsymbol{f} \end{cases} \tag{2}$$

where $\boldsymbol{x} = [\boldsymbol{\gamma}^{\mathrm{T}}, \boldsymbol{\zeta}^{\mathrm{T}}]^{\mathrm{T}}$, $\boldsymbol{y} = [\boldsymbol{\omega}^{\mathrm{T}}, \boldsymbol{\upsilon}^{\mathrm{T}}]^{\mathrm{T}}$, $\boldsymbol{R} = \mathrm{diag}\{\boldsymbol{R}_\gamma(\boldsymbol{\gamma}), \boldsymbol{R}_g(\boldsymbol{\gamma})\}$, $\boldsymbol{N}_1 = [n_1, n_2, \cdots, n_6]^{\mathrm{T}}$, $\boldsymbol{N}_2^* = [-z_g mg\cos\theta\sin\phi, -z_g mg\sin\theta - x_g mg\cos\theta\cos\phi, x_g mg\cos\theta\sin\phi, (B_f - mg)\sin\theta, -(B_f - mg)\cos\theta\sin\phi, -(B_f - mg)\cos\theta\cos\phi]^{\mathrm{T}}$,

$$\boldsymbol{R}_\gamma(\boldsymbol{\gamma}) = \begin{bmatrix} 1 & \sin\phi\tan\theta & \cos\phi\tan\theta \\ 0 & \cos\phi & -\sin\phi \\ 0 & \dfrac{\sin\phi}{\cos\theta} & \dfrac{\cos\phi}{\cos\theta} \end{bmatrix},$$

$$\boldsymbol{M} = \begin{bmatrix} I_x & 0 & -I_{xz} & 0 & -mz_g & 0 \\ 0 & \bar{I}_y & 0 & mz_g & 0 & -mx_g \\ -I_{xz} & 0 & \bar{I}_z & 0 & mx_g & 0 \\ 0 & mz_g & 0 & \bar{m}_x & 0 & 0 \\ -mz_g & 0 & mx_g & 0 & \bar{m}_y & 0 \\ 0 & -mx_g & 0 & 0 & 0 & \bar{m}_y \end{bmatrix},$$

$$\boldsymbol{B} = \begin{bmatrix} \cos\mu & \cos\mu & 0 & 0 & 0 & 0 \\ \sin\mu & -\sin\mu & 0 & 0 & 0 & b_5 \\ 0 & 0 & 1 & 1 & b_3 & 0 \\ -z_p\sin\mu & -z_p\sin\mu & y_p & -y_p & 0 & 0 \\ z_p\sin\mu & z_p\cos\mu & -x_p & -x_p & b_4 & 0 \\ b_1 & b_2 & 0 & 0 & 0 & b_6 \end{bmatrix},$$

$\alpha = \mathrm{arctan2}(w, u)$, $\beta = \mathrm{arctan2}(v\cos\alpha, u)$, $\bar{I}_y = I_y + \rho\nabla k_3'$, $\bar{I}_z = I_z + \rho\nabla k_3'$, $\bar{m}_x = m + \rho\nabla k_1'$, $\bar{m}_y = m + \rho\nabla k_2'$, $n_1 = -(I_z - I_y)qr + I_{xz}pq + mz_g(ur - wp)$, $n_2 = -(I_x - I_z - \rho\nabla k_3')pr - I_{xz}(p^2 - r^2) - mz_g(wq - vr) + mx_g(vp - uq)$, $n_3 = -(I_y + \rho\nabla k_3' - I_x)pq - I_{xz}qr - mx_g(ur - wp)$, $n_4 = -(m+\rho\nabla k_2')(wq - vr) + mx_g(q^2 + r^2) - mz_g pr$, $n_5 = (m+\rho\nabla k_2')wp - (m+\rho\nabla k_1')ur - mx_g pq - mz_g qr$, $n_6 = (m + \rho\nabla k_1')uq - (m + \rho\nabla k_2')vp - mx_g rp + mz_g(q^2 + p^2)$, $b_1 = x_p\sin\mu - y_p\cos\mu$, $b_2 = x_p\sin\mu + y_p\cos\mu$, $b_3 = -2l_pC_{n4}$, $b_4 = 2l_pC_{y4}$, $b_5 = -2l_pC_{m4}$, $b_6 = -2l_pC_{z4}$; $\boldsymbol{\tau} \in \mathbb{R}^6$ is the six-degrees-of-freedom control inputs of the airship, where $\{u_1, u_2, u_3, u_4\}$ represent the propulsive forces and $\{u_5, u_6\}$ are the elevator and rudder control deflections; $\boldsymbol{f} \in \mathbb{R}^6$ is the unknown wind disturbance; m is the airship's mass; $\{I_x, I_y, I_z\}$ and I_{xz} are the moments of inertia and products of inertia respectively; ∇ is the airship's volume; x_g and z_g are the coordinates of the CG; $\{k_1', k_2', k_3'\}$ are the ellipsoid inertia factors; $l_p = \rho V^2/2$ is the dynamic pressure, ρ is the air density at the flight altitude and $V = \sqrt{u^2 + v^2 + w^2}$ is the airship speed; $C_{ij}(i = l, m, n, x, y, z; j = 1, 2, 3, 4)$ represent the aerodynamic coefficients of the airship; B_f is the buoyancy force; g is earth's gravitational acceleration; $\{x_p, y_p, z_p\}$ defines the propeller position in BRF; μ is the angle of the propellers with respect to Oxz plane.

Assumption 1. The aero-elastic effects of airship are ignored that renders the airship to be viewed as a rigid body. The center volume and the center of buoyancy for the airship are coincident, indicating that the airship is always kept in the neutral buoyant state, such that $B_f = mg$.

Assumption 2. The position and velocities $\{\boldsymbol{\gamma}, \boldsymbol{\zeta}, \boldsymbol{\omega}, \boldsymbol{\upsilon}\}$ are measurable. $\boldsymbol{\zeta}_c$ is differentiable and its corresponding derivatives $\{\dot{\boldsymbol{\zeta}}_c, \ddot{\boldsymbol{\zeta}}_c, \boldsymbol{\zeta}_c^{(3)}, \boldsymbol{\zeta}_c^{(4)}\}$ are bounded. The attitude $\boldsymbol{\gamma}$ satisfies $|\theta| < \pi/2$, such that $\boldsymbol{R}_\gamma(\boldsymbol{\gamma})$ in (2) is always nonsingular. In the overall design of the stratospheric airship, the appropriate installation parameters $\{\mu, x_p, y_p, z_p\}$ of the propellers have been chosen such that the matrix $\boldsymbol{B}$ in (2) is invertible.

For the external disturbances, the stratosphere's wind field and the airship's flight speed are in the same order of magnitude, resulting in non-negligible impact. In addition, the stratosphere environment's parameters, such as density, temperature and pressure, have a complicated multi-physics coupling effect on the airship. For example, the airship's buoyancy will be affected if there is a thermodynamic change in the environment. Since these complex effects are difficult to modeled or measured in real time, these effects are referred as the lump capacitance $\boldsymbol{f}$ in the airship's equation. Although the magnitude of $\boldsymbol{f}$ is unknown, the disturbance $\boldsymbol{f}$ that includes wind field and uncertainties cannot be infinitely large. Therefore, it is reasonable to assume that $\boldsymbol{f}$ is bounded.

Assumption 3. The external disturbance vector $\boldsymbol{f}$ is unknown but bounded by an unknown vector $\boldsymbol{\sigma}$ such that $|f_i| \leq \sigma_i (i = 1, 2, \cdots, 6)$.

2.3. Control objective and coordinate transformation

In this paper, the control objective is to design the control input $\boldsymbol{\tau}$ under the Assumptions 1–3, such that the trajectory of the airship, in the presence of unknown disturbances, $\boldsymbol{f}$ successfully tracks the desired trajectory $\boldsymbol{\zeta}_c$ in a fixed-time.

Before initiating the control design, we are first required to generate the desired attitude from the desired trajectory $\boldsymbol{\zeta}_c$. The

$$\boldsymbol{R}_g(\boldsymbol{\gamma}) = \begin{bmatrix} \cos\theta\cos\psi & \sin\theta\cos\psi\sin\phi - \sin\psi\cos\phi & \sin\theta\cos\psi\cos\phi + \sin\psi\sin\phi \\ \cos\theta\sin\psi & \sin\theta\sin\psi\sin\phi + \cos\psi\cos\phi & \sin\theta\sin\psi\cos\phi - \cos\psi\sin\phi \\ -\sin\theta & \cos\theta\sin\phi & \cos\theta\cos\phi \end{bmatrix};$$

$$\boldsymbol{N}_3 = \begin{bmatrix} l_p C_{l1}\sin\beta\sin|\beta| \\ -l_p\left(C_{m1}\cos(\alpha/2)\sin(2\alpha) + C_{m2}\sin(2\alpha) + C_{m3}\sin\alpha\sin|\alpha|\right) \\ l_p\left(C_{n1}\cos(\beta/2)\sin(2\beta) + C_{n2}\sin(2\beta) + C_{n3}\sin\beta\sin|\beta|\right) \\ -l_p\left(C_{x1}\cos^2\alpha\cos^2\beta + C_{x2}\sin(2\alpha)\sin(\alpha/2)\right) \\ -l_p\left(C_{y1}\cos(\beta/2)\sin(2\beta) + C_{y2}\sin(2\beta) + C_{y3}\sin\beta\sin|\beta|\right) \\ -l_p\left(C_{z1}\cos(\alpha/2)\sin(2\alpha) + C_{z2}\sin(2\alpha) + C_{z3}\sin\alpha\sin|\alpha|\right) \end{bmatrix},$$

desired attitude of the airship is expressed by using the Frenet frame which involves the use of the unit vectors of the desired trajectory $\boldsymbol{\zeta}_c(t)$ shown below [12].

$$\boldsymbol{e}_t = \frac{\dot{\boldsymbol{\zeta}}_c}{\|\dot{\boldsymbol{\zeta}}_c\|},\ \ \boldsymbol{e}_b = \frac{\dot{\boldsymbol{\zeta}}_c \times \ddot{\boldsymbol{\zeta}}_c}{\|\dot{\boldsymbol{\zeta}}_c \times \ddot{\boldsymbol{\zeta}}_c\|},\ \ \boldsymbol{e}_n = \boldsymbol{e}_b \times \boldsymbol{e}_t. \tag{3}$$

As $\boldsymbol{e}_n$ always points towards the concave side of trajectory $\boldsymbol{\zeta}_c$ rather than the right side of the airship's body, the desired trajectory $\boldsymbol{\zeta}_c$ should be designed such that $e_{b3} \neq 0$ (e_{b3} is the third entry of unit vector $\boldsymbol{e}_b$) to avoid this drawback. The desired reference frame can be constructed using $\{\boldsymbol{e}_t, \mathrm{sgn}(e_{b3})\boldsymbol{e}_n, \mathrm{sgn}(e_{b3})\boldsymbol{e}_b\}$, where $\mathrm{sgn}(e_{b3})$ represents the signum function for e_{b3}. Then, the rotation matrix between the desired reference frame to ERF is described as $\boldsymbol{R}_g^c = [\boldsymbol{e}_t, \mathrm{sgn}(e_{b3})\boldsymbol{e}_n, \mathrm{sgn}(e_{b3})\boldsymbol{e}_b]$. Comparing $\boldsymbol{R}_g^c = [r_{ij}](i = j = 1, 2, 3)$ with $\boldsymbol{R}_g$ would result in the desired attitude $\boldsymbol{\gamma}_c = [\phi_c, \theta_c, \psi_c]^{\mathrm{T}}$ where

$$\phi_c = \arctan\left(\frac{r_{32}}{r_{33}}\right), \theta_c = \arctan\left(\frac{-r_{31}}{\sqrt{r_{11}^2 + r_{21}^2}}\right),$$

$$\psi_c = \arctan\left(\frac{r_{21}}{r_{11}}\right).$$

The desired angular rates $\{\dot{\boldsymbol{\gamma}}_c, \ddot{\boldsymbol{\gamma}}_c\}$ are conveniently derived by computing the derivatives of $\boldsymbol{\gamma}_c$ directly.

Based on the equations $\boldsymbol{R}_g^{-1} = \boldsymbol{R}_g^{\mathrm{T}}$ and $\dot{\boldsymbol{R}}_g(\boldsymbol{\gamma}_c) = \boldsymbol{R}_g(\boldsymbol{\gamma}_c)S(\boldsymbol{\omega}_c)$, the desired velocities and accelerations are expressed as

$$\begin{cases} \boldsymbol{\omega}_c = \boldsymbol{R}_\gamma^{-1}(\boldsymbol{\gamma}_c)\dot{\boldsymbol{\gamma}}_c \triangleq [p_c, q_c, r_c]^{\mathrm{T}} \\ \dot{\boldsymbol{\omega}}_c = \boldsymbol{R}_\gamma^{-1}(\boldsymbol{\gamma}_c)(\ddot{\boldsymbol{\gamma}}_c - \dot{\boldsymbol{R}}_\gamma(\boldsymbol{\gamma}_c)\boldsymbol{\omega}_c) \\ \boldsymbol{\upsilon}_c = \boldsymbol{R}_g^{\mathrm{T}}(\boldsymbol{\gamma}_c)\dot{\boldsymbol{\zeta}}_c \\ \dot{\boldsymbol{\upsilon}}_c = \boldsymbol{R}_g^{\mathrm{T}}(\boldsymbol{\gamma}_c)(\ddot{\boldsymbol{\zeta}}_c - \boldsymbol{R}_g(\boldsymbol{\gamma}_c)S(\boldsymbol{\omega}_c)\boldsymbol{\upsilon}_c) \end{cases} \tag{4}$$

where

$$\boldsymbol{R}_\gamma^{-1}(\boldsymbol{\gamma}_c) = \begin{bmatrix} 1 & 0 & -\sin\theta_c \\ 0 & \cos\phi_c & \sin\phi_c\cos\theta_c \\ 0 & -\sin\phi_c & \cos\phi_c\cos\theta_c \end{bmatrix}, S(\boldsymbol{\omega}_c) = \begin{bmatrix} 0 & -r_c & q_c \\ r_c & 0 & -p_c \\ -q_c & p_c & 0 \end{bmatrix},$$

$$\dot{\boldsymbol{R}}_\gamma(\boldsymbol{\gamma}_c) = \begin{bmatrix} 0 & \frac{\dot{\theta}_c\sin\phi_c + \dot{\phi}_c\tan\theta_c\cos\phi_c}{\cos^2\theta_c} & \frac{\dot{\theta}_c\sin\phi_c - \dot{\phi}_c\tan\theta_c\sin\phi_c}{\cos^2\theta_c} \\ 0 & -\dot{\phi}_c\sin\phi_c & -\dot{\phi}_c\cos\phi_c \\ 0 & \frac{\dot{\phi}_c\cos\phi_c\cos\theta_c + \dot{\theta}_c\sin\phi_c\sin\theta_c}{\cos^2\theta_c} & \frac{-\dot{\phi}_c\sin\phi_c\cos\theta_c + \dot{\theta}_c\cos\phi_c\sin\theta_c}{\cos^2\theta_c} \end{bmatrix}.$$

Due to $B_f = mg$ in Assumption 1, $\boldsymbol{N}_2^*$ in (2) can be simplified to $\boldsymbol{N}_2 = [-z_g mg\cos\theta\sin\phi, -z_g mg\sin\theta - x_g mg\cos\theta\cos\phi, x_g mg\cos\theta\sin\phi, 0, 0, 0]^{\mathrm{T}}$. Subsequently, the trajectory tracking model can be derived as

$$\begin{cases} \dot{\boldsymbol{x}}_e = (\boldsymbol{R} - \boldsymbol{R}_c)\boldsymbol{y}_c + \boldsymbol{R}\boldsymbol{y}_e \\ \boldsymbol{M}\dot{\boldsymbol{y}}_e = \boldsymbol{N}_1 + \boldsymbol{N}_2 + \boldsymbol{N}_3 + \boldsymbol{B}\boldsymbol{\tau} + \boldsymbol{f} - \boldsymbol{M}\dot{\boldsymbol{y}}_c \end{cases} \tag{5}$$

where $\boldsymbol{x}_e = \boldsymbol{x} - \boldsymbol{x}_c$, $\boldsymbol{y}_e = \boldsymbol{y} - \boldsymbol{y}_c$, $\boldsymbol{x}_c = [\boldsymbol{\gamma}_c^{\mathrm{T}}, \boldsymbol{\zeta}_c^{\mathrm{T}}]^{\mathrm{T}}$, $\boldsymbol{y}_c = [\boldsymbol{\omega}_c^{\mathrm{T}}, \boldsymbol{\upsilon}_c^{\mathrm{T}}]^{\mathrm{T}}$ and $\boldsymbol{R}_c = \mathrm{diag}\{\boldsymbol{R}_\gamma(\boldsymbol{\gamma}_c), \boldsymbol{R}_g(\boldsymbol{\gamma}_c)\}$.

By defining $z_1 = \boldsymbol{x}_e$, $z_2 = \dot{\boldsymbol{x}}_e$, (5) can thereafter be described as

$$\begin{cases} \dot{z}_1 = z_2 \\ \dot{z}_2 = \boldsymbol{C}(z_1, z_2) + \boldsymbol{R}\boldsymbol{M}^{-1}\boldsymbol{B}\boldsymbol{\tau} + \boldsymbol{R}\boldsymbol{M}^{-1}\boldsymbol{f} \end{cases} \tag{6}$$

where $\boldsymbol{C}(z_1, z_2) = \dot{\boldsymbol{R}}\boldsymbol{R}^{-1}z_2 - \dot{\boldsymbol{R}}\boldsymbol{R}^{-1}(\boldsymbol{R} - \boldsymbol{R}_c)\boldsymbol{y}_c + (\dot{\boldsymbol{R}} - \dot{\boldsymbol{R}}_c)\boldsymbol{y}_c + (\boldsymbol{R} - \boldsymbol{R}_c)\dot{\boldsymbol{y}}_c + \boldsymbol{R}\boldsymbol{M}^{-1}(\boldsymbol{N}_1 + \boldsymbol{N}_2 + \boldsymbol{N}_3 - \boldsymbol{M}\dot{\boldsymbol{y}}_c)$.

Based on the formulated tracking error dynamics (6), the control objective of trajectory tracking will be achieved by designing the control law $\boldsymbol{\tau}$ such that the transformed tracking errors $\boldsymbol{z}_1$ and $\boldsymbol{z}_2$ are sufficiently small within a fixed time.

3. Fixed-time control design

3.1. Fixed-time control without disturbances

We first design the fixed-time trajectory tracking controller based on the framework where external disturbances are not taken into account, i.e. $\boldsymbol{f} = \boldsymbol{0}$. Based on (6), the input signal is designed as

$$\begin{aligned} \boldsymbol{\tau} = -\boldsymbol{B}^{-1}\boldsymbol{M}\boldsymbol{R}^{-1}\Big(&\lceil\boldsymbol{\xi}^{2\varphi-1}\rfloor(\boldsymbol{k}_3 + \lceil\boldsymbol{k}_4\rfloor\boldsymbol{\xi}^{\varrho}) + \boldsymbol{C}(z_1, z_2) \\ &+ \lceil\bar{\boldsymbol{\chi}}\rfloor\boldsymbol{\xi}^{2\varphi-1} + \frac{2^{1-\varphi}\iota^{-\frac{1}{\varphi}}\varphi}{1+\varphi}\boldsymbol{\xi}^{2\varphi-1}\Big) \end{aligned} \tag{7}$$

where $\boldsymbol{\xi} = z_2^{\frac{1}{\varphi}} - z_{2c}^{\frac{1}{\varphi}}$, $z_{2c} = -\lceil z_1^{\varphi}\rfloor(\boldsymbol{k}_1 + \lceil\boldsymbol{k}_2\rfloor z_1^{\varrho})$, $\bar{\boldsymbol{\chi}} = 2^{1-\varphi}(2 - \varphi)(\frac{\iota^{-\frac{1}{\varphi}}\varphi}{1+\varphi}(\lceil\boldsymbol{\chi}\rfloor(\boldsymbol{k}_1 + \lceil\boldsymbol{k}_2\rfloor z_1^{\varrho}))^{1+\varphi} + \boldsymbol{\chi})$, $\boldsymbol{\chi} = (\boldsymbol{k}_1 + \lceil\boldsymbol{k}_2\rfloor z_1^{\varrho})^{\frac{1}{\varphi}} + \frac{\varrho}{\varphi}\lceil\boldsymbol{k}_2\rfloor\lceil z_1^{\varrho}\rfloor(\boldsymbol{k}_1 + \lceil\boldsymbol{k}_2\rfloor z_1^{\varrho})^{\frac{1}{\varphi}-1}$, $\varphi = \varphi_1/\varphi_2 \in (0, 1)$, $\varrho = \varrho_1/\varrho_2 > 1$, with $\varphi_1, \varphi_2, \varrho_2$ being odd integers and ϱ_1 being an even integer; $\iota > 0$; $\boldsymbol{k}_j \in \mathbb{R}^6, j = 1, \cdots, 4$ is the control parameter vector which satisfies

$$k_{1i} > \frac{2^{1-\varphi}(3-\varphi)\iota}{1+\varphi}, k_{2i} > 0, k_{3i} > 0, k_{4i} > 0. \tag{8}$$

Having established the above formulae, the following theorem is presented.

Theorem 1. *Consider the stratospheric airship* (2) *under Assumption 1-2. If the control input is designed as* (7) *and there are no disturbances, then the desired trajectory $\boldsymbol{\zeta}_c$ will be exactly tracked within a fixed time.*

Proof. We will obtain the proof process by employing the method of adding a power integrator recursively [26, 28]. Firstly, consider the Lyapunov function candidate $V_0 = \frac{1}{2}z_1^T z_1$ for the z_1-subsystem of (6). Using (7) and Lemmas 4-5, we determine the derivative of V_0 to be

$$\begin{aligned}\dot{V}_0 =& z_1^T z_{2c} + z_1^T(z_2 - z_{2c})\\ \leq& -\sum_{i=1}^{6} k_{1i} z_{1i}^{1+\varphi} - \sum_{i=1}^{6} k_{2i} z_{1i}^{\bar{\varrho}} + 2^{1-\varphi}\sum_{i=1}^{6}|z_{1i}||\xi_i|^{\varphi}\\ \leq& -\sum_{i=1}^{6}\Big(k_{1i} - \frac{2^{1-\varphi}\iota}{1+\varphi}\Big)z_{1i}^{1+\varphi} - \sum_{i=1}^{6} k_{2i} z_{1i}^{\bar{\varrho}}\\ &+ \frac{2^{1-\varphi}\iota^{-\frac{1}{\varphi}}\varphi}{1+\varphi}\sum_{i=1}^{6}\xi_i^{1+\varphi}\end{aligned}$$

where $\bar{\varrho} = 1 + \varphi + \varrho$. Thereafter, we select the complete Lyapunov function candidate as

$$V_1 = V_0 + \sum_{i=1}^{6}\int_{z_{2ci}}^{z_{2i}}\left(s^{\frac{1}{\varphi}} - z_{2ci}^{\frac{1}{\varphi}}\right)^{2-\varphi}\mathrm{d}s. \tag{9}$$

From [28], V_1 has been shown to be positive definite. To carry out the stability analyses, we utilize the following derivations

$$\begin{aligned}\Big|\frac{\mathrm{d}(z_{2ci}^{\frac{1}{\varphi}})}{\mathrm{d}t}\Big| &= \Big|\frac{\partial(z_{2ci}^{\frac{1}{\varphi}})}{\partial z_{1i}}\Big||z_{2i}| = \chi_i|z_{2i}|\\ &\leq \chi_i(|\xi_i|^{\varphi} + |z_{1i}|^{\varphi}(k_{1i} + k_{2i}z_{1i}^{\varrho}))\end{aligned}$$

and

$$\int_{z_{2ci}}^{z_{2i}}(s^{\frac{1}{\varphi}} - z_{2ci}^{\frac{1}{\varphi}})^{1-\varphi}\mathrm{d}s \leq |z_{2i} - z_{2ci}|\xi_i^{1-\varphi} \leq 2^{1-\varphi}|\xi_i|.$$

Accordingly, it yields that

$$\begin{aligned}&-(2-\varphi)\frac{\mathrm{d}(z_{2ci}^{\frac{1}{\varphi}})}{\mathrm{d}t}\int_{z_{2ci}}^{z_{2i}}(s^{\frac{1}{\varphi}} - z_{2ci}^{\frac{1}{\varphi}})^{1-\varphi}\mathrm{d}s\\ &\leq 2^{1-\varphi}(2-\varphi)(|\xi_i|^{1+\varphi}\chi_i + |z_{1i}|^{\varphi}|\xi_i|\chi_i(k_{1i} + k_{2i}z_{1i}^{\varrho}))\\ &\leq \frac{2^{1-\varphi}(2-\varphi)\iota}{1+\varphi}z_{1i}^{1+\varphi} + \bar{\chi}_i\xi_i^{1+\varphi}.\end{aligned}$$

Therefore, the derivative of V_1 satisfies

$$\begin{aligned}\dot{V}_1 =& \dot{V}_0 + \sum_{i=1}^{6}\xi_i^{2-\varphi}\dot{z}_{2i} - (2-\varphi)\sum_{i=1}^{6}\frac{\mathrm{d}(z_{2ci}^{\frac{1}{\varphi}})}{\mathrm{d}t}\int_{z_{2ci}}^{z_{2i}}(s^{\frac{1}{\varphi}} - z_{2ci}^{\frac{1}{\varphi}})^{1-\varphi}\mathrm{d}s\\ \leq& -\sum_{i=1}^{6}\Big(k_{1i} - \frac{2^{1-\varphi}(3-\varphi)\iota}{1+\varphi}\Big)z_{1i}^{1+\varphi} - \sum_{i=1}^{6}k_{2i}z_{1i}^{\bar{\varrho}}\\ &+ \frac{2^{1-\varphi}\iota^{-\frac{1}{\varphi}}\varphi}{1+\varphi}\sum_{i=1}^{6}\xi_i^{1+\varphi} + \sum_{i=1}^{6}\bar{\chi}_i\xi_i^{1+\varphi} + \sum_{i=1}^{6}\xi_i^{2-\varphi}\dot{z}_{2i}\\ \leq& -\sum_{i=1}^{6}\Big(k_{1i} - \frac{2^{1-\varphi}(3-\varphi)\iota}{1+\varphi}\Big)z_{1i}^{1+\varphi} - \sum_{i=1}^{6}k_{2i}z_{1i}^{\bar{\varrho}}\\ &- \sum_{i=1}^{6}k_{3i}\xi_i^{1+\varphi} - \sum_{i=1}^{6}k_{4i}\xi_i^{\bar{\varrho}}.\end{aligned} \tag{10}$$

From Lemma 5, we obtain

$$\begin{aligned}V_1 \leq& \frac{1}{2}\sum_{i=1}^{6}z_{1i}^2 + \sum_{i=1}^{6}|z_{2i} - z_{2ci}|\xi_i^{2-\varphi}\\ \leq& \frac{1}{2}\sum_{i=1}^{6}z_{1i}^2 + 2^{1-\varphi}\sum_{i=1}^{6}\xi_i^2\\ \leq& 2\sum_{i=1}^{6}z_{1i}^2 + 2\sum_{i=1}^{6}\xi_i^2\end{aligned} \tag{11}$$

Then, the following holds

$$\begin{aligned}&V_1^{\frac{1+\varphi}{2}} \leq 2^{\frac{1+\varphi}{2}}\sum_{i=1}^{6}z_{1i}^{1+\varphi} + 2^{\frac{1+\varphi}{2}}\sum_{i=1}^{6}\xi_i^{1+\varphi}\\ \Rightarrow& -k_{\varphi}\sum_{i=1}^{6}z_{1i}^{1+\varphi} - k_{\varphi}\sum_{i=1}^{6}\xi_i^{1+\varphi} \leq -2^{-\frac{1+\varphi}{2}}k_{\varphi}V_1^{\frac{1+\varphi}{2}}\end{aligned} \tag{12}$$

where $k_{\varphi} = \min\{k_{1i} - \frac{2^{1-\varphi}(3-\varphi)\iota}{1+\varphi}, k_{3i}\}$. On the other hand, it can be deduced from (11) and Lemma 5 that

$$\begin{aligned}&\sum_{i=1}^{6}z_{1i}^{\bar{\varrho}} + \sum_{i=1}^{6}\xi_i^{\bar{\varrho}} \geq 2^{-\frac{\bar{\varrho}}{2}}12^{\frac{1-\varphi-\varrho}{2}}V_1^{\frac{\bar{\varrho}}{2}}\\ \Rightarrow& -k_{\varrho}\sum_{i=1}^{6}z_{1i}^{\bar{\varrho}} - k_{\varrho}\sum_{i=1}^{6}\xi_i^{\bar{\varrho}} \leq -2^{-\frac{\bar{\varrho}}{2}}12^{\frac{1-\varphi-\varrho}{2}}k_{\varrho}V_1^{\frac{\bar{\varrho}}{2}}\end{aligned} \tag{13}$$

where $k_{\varrho} = \min\{k_{2i}, k_{4i}\}$. Consequently, (10) becomes

$$\dot{V}_1 \leq -2^{-\frac{1+\varphi}{2}}k_{\varphi}V_1^{\frac{1+\varphi}{2}} - 2^{-\frac{\bar{\varrho}}{2}}12^{\frac{1-\varphi-\varrho}{2}}k_{\varrho}V_1^{\frac{\bar{\varrho}}{2}}. \tag{14}$$

Since (14) is in expressed in the form that satisfies Lemma 1, the origin of (6) is therefore proven to be fixed-time stable. The setting time is bounded by a positive constant T_{max} which is independent of the initial conditions of the airship. □

3.2. Adaptive fixed-time control with disturbances

In this section, the complete adaptive controller for the stratospheric airship is formulated to handle the presence of external

disturbance $\boldsymbol{f}$. The control input and adaptive law are chosen as

$$\begin{aligned}\boldsymbol{\tau} =&-\boldsymbol{B}^{-1}\boldsymbol{M}\boldsymbol{R}^{-1}\Big(\lceil\boldsymbol{\xi}^{2\varrho-1}\rfloor(\boldsymbol{k}_3+\lceil\boldsymbol{k}_4\rfloor\boldsymbol{\xi}^{\varrho})+\boldsymbol{C}(z_1,z_2)\\&+\lceil\bar{\boldsymbol{\chi}}\rfloor\boldsymbol{\xi}^{2\varphi-1}+\frac{2^{1-\varphi}\iota^{-\frac{1}{\varphi}}\varphi}{1+\varphi}\boldsymbol{\xi}^{2\varphi-1}\Big)-\boldsymbol{B}^{-1}\mathrm{Tanh}\Big(\frac{\boldsymbol{\Omega}}{\eta}\Big)\hat{\boldsymbol{\sigma}}\end{aligned}\tag{15}$$

$$\dot{\hat{\boldsymbol{\sigma}}} =\mathrm{Tanh}\Big(\frac{\boldsymbol{\Omega}}{\eta}\Big)\boldsymbol{\Omega}-k_\sigma\hat{\boldsymbol{\sigma}}\tag{16}$$

where $\boldsymbol{\Omega}=(\boldsymbol{M}^{-1})^T\boldsymbol{R}^T\boldsymbol{\xi}^{2-\varphi}$, $k_\sigma>0$. Based on the above formulations, the following theorem is detailed.

Theorem 2. *Consider the stratospheric airship* (2) *under Assumption 1-3. If the input signal is designed as* (15) *under the adaptive law* (16)*, then the desired trajectory $\boldsymbol{\zeta}_c$ will converge to a residual set within a fixed time.*

Proof. Consider the Lyapunov function candidate $V_2=V_1+\frac{1}{2}\tilde{\boldsymbol{\sigma}}^T\tilde{\boldsymbol{\sigma}}$, where $\tilde{\boldsymbol{\sigma}}=\hat{\boldsymbol{\sigma}}-\boldsymbol{\sigma}$. Then, from (10)-(14), the derivative of V_2 satisfies

$$\begin{aligned}\dot{V}_2\le&-k_\varphi\sum_{i=1}^{6}z_{1i}^{1+\varphi}-k_\varphi\sum_{i=1}^{6}z_{1i}^{\bar{\varrho}}-k_\varrho\sum_{i=1}^{6}\xi_i^{1+\varphi}-k_\varrho\sum_{i=1}^{6}\xi_i^{\bar{\varrho}}\\&-\boldsymbol{\Omega}^T\mathrm{Tanh}\Big(\frac{\boldsymbol{\Omega}}{\eta}\Big)\hat{\boldsymbol{\sigma}}+\boldsymbol{\Omega}^T\boldsymbol{f}+\tilde{\boldsymbol{\sigma}}^T\dot{\hat{\boldsymbol{\sigma}}}\end{aligned}\tag{17}$$

From Lemma 3 and Assumption 3, we can obtain

$$\begin{aligned}\boldsymbol{\Omega}^T\boldsymbol{f}\le&\sum_{i=1}^{6}|\Omega_i|\sigma_i\le\sum_{i=1}^{6}\Big(\Omega_i\tanh\Big(\frac{\Omega_i}{\eta}\Big)\sigma_i+\kappa\eta\sigma_i\Big)\\=&\boldsymbol{\Omega}^T\mathrm{Tanh}\Big(\frac{\boldsymbol{\Omega}}{\eta}\Big)\boldsymbol{\sigma}+\sigma_f,\end{aligned}$$

where $\sigma_f=\sum_{i=1}^{6}\kappa\eta\sigma_i$. Then, (17) becomes

$$\begin{aligned}\dot{V}_2\le&-k_\varphi\sum_{i=1}^{6}z_{1i}^{1+\varphi}-k_\varphi\sum_{i=1}^{6}z_{1i}^{\bar{\varrho}}-k_\varrho\sum_{i=1}^{6}\xi_i^{1+\varphi}-k_\varrho\sum_{i=1}^{6}\xi_i^{\bar{\varrho}}\\&-k_\sigma\tilde{\boldsymbol{\sigma}}^T\hat{\boldsymbol{\sigma}}+\sigma_f\end{aligned}\tag{18}$$

By using Young's inequality, it yields

$$\begin{aligned}-k_\sigma\tilde{\boldsymbol{\sigma}}^T\hat{\boldsymbol{\sigma}}=&-k_\sigma\tilde{\boldsymbol{\sigma}}^T(\tilde{\boldsymbol{\sigma}}+\boldsymbol{\sigma})\\\le&-k_\sigma\tilde{\boldsymbol{\sigma}}^T\tilde{\boldsymbol{\sigma}}+\frac{k_\sigma}{2}\tilde{\boldsymbol{\sigma}}^T\tilde{\boldsymbol{\sigma}}+\frac{k_\sigma}{2}\boldsymbol{\sigma}^T\boldsymbol{\sigma}\\\le&-\frac{k_\sigma}{2}\tilde{\boldsymbol{\sigma}}^T\tilde{\boldsymbol{\sigma}}+\frac{k_\sigma}{2}\boldsymbol{\sigma}^T\boldsymbol{\sigma}\\\le&-\Big(\frac{k_\sigma\delta_0}{2}\tilde{\boldsymbol{\sigma}}^T\tilde{\boldsymbol{\sigma}}\Big)^{\frac{1+\varphi}{2}}-\Big(\frac{k_\sigma\delta_0}{2}\tilde{\boldsymbol{\sigma}}^T\tilde{\boldsymbol{\sigma}}\Big)^{\frac{\bar{\varrho}}{2}}\\&+\Big(\frac{k_\sigma\delta_0}{2}\tilde{\boldsymbol{\sigma}}^T\tilde{\boldsymbol{\sigma}}\Big)^{\frac{1+\varphi}{2}}+\Big(\frac{k_\sigma\delta_0}{2}\tilde{\boldsymbol{\sigma}}^T\tilde{\boldsymbol{\sigma}}\Big)^{\frac{\bar{\varrho}}{2}}\\&-\delta_0^{\frac{1+\varphi}{2}}\frac{k_\sigma}{2}\tilde{\boldsymbol{\sigma}}^T\tilde{\boldsymbol{\sigma}}-\Big(1-\delta_0^{\frac{1+\varphi}{2}}\Big)\frac{k_\sigma}{2}\tilde{\boldsymbol{\sigma}}^T\tilde{\boldsymbol{\sigma}}+\frac{k_\sigma}{2}\boldsymbol{\sigma}^T\boldsymbol{\sigma}\end{aligned}$$

Denote that $\delta_0=1-\delta_0^{\frac{1+\varphi}{2}}$. Hence, if $\frac{k_\sigma}{2}\tilde{\boldsymbol{\sigma}}^T\tilde{\boldsymbol{\sigma}}\ge1$, we have $(\frac{k_\sigma}{2}\tilde{\boldsymbol{\sigma}}^T\tilde{\boldsymbol{\sigma}})^{\frac{1+\varphi}{2}}-\frac{k_\sigma}{2}\tilde{\boldsymbol{\sigma}}^T\tilde{\boldsymbol{\sigma}}\le0$. Otherwise, if $\frac{k_\sigma}{2}\tilde{\boldsymbol{\sigma}}^T\tilde{\boldsymbol{\sigma}}<1$, we have $(\frac{k_\sigma}{2}\tilde{\boldsymbol{\sigma}}^T\tilde{\boldsymbol{\sigma}})^{\frac{1+\varphi}{2}}-\frac{k_\sigma}{2}\tilde{\boldsymbol{\sigma}}^T\tilde{\boldsymbol{\sigma}}<\Phi_1$, where $\Phi_1=\varphi_1^{\frac{\varphi_1}{1-\varphi_1}}-\varphi_1^{\frac{1}{1-\varphi_1}}$, $\varphi_1=(1+\varphi)/2$. This means that $(\frac{k_\sigma\delta_0}{2}\tilde{\boldsymbol{\sigma}}^T\tilde{\boldsymbol{\sigma}})^{\frac{1+\varphi}{2}}-\delta_0^{\frac{1+\varphi}{2}}\frac{k_\sigma}{2}\tilde{\boldsymbol{\sigma}}^T\tilde{\boldsymbol{\sigma}}<\delta_0^{\frac{1+\varphi}{2}}\Phi_1$. Moreover, if $\|\tilde{\boldsymbol{\sigma}}\|\le\Delta$ and $\Delta<\sqrt{2/(k_\sigma\delta_0)}$, we obtain $(\frac{k_\sigma\delta_0}{2}\tilde{\boldsymbol{\sigma}}^T\tilde{\boldsymbol{\sigma}})^{\frac{\bar{\varrho}}{2}}-\frac{k_\sigma\delta_0}{2}\tilde{\boldsymbol{\sigma}}^T\tilde{\boldsymbol{\sigma}}<0$. Otherwise, if $\Delta\ge\sqrt{2/(k_\sigma\delta_0)}$, we obtain $(\frac{k_\sigma\delta_0}{2}\tilde{\boldsymbol{\sigma}}^T\tilde{\boldsymbol{\sigma}})^{\frac{\bar{\varrho}}{2}}-\frac{k_\sigma\delta_0}{2}\tilde{\boldsymbol{\sigma}}^T\tilde{\boldsymbol{\sigma}}\le(\frac{k_\sigma\delta_0}{2}\Delta^2)^{\frac{\bar{\varrho}}{2}}-\frac{k_\sigma\delta_0}{2}\Delta^2$. Therefore, (18) can be rewritten as

$$\begin{aligned}\dot{V}_2\le&-k_\varphi\sum_{i=1}^{6}z_{1i}^{1+\varphi}-k_\varphi\sum_{i=1}^{6}z_{1i}^{\bar{\varrho}}-k_\varrho\sum_{i=1}^{6}\xi_i^{1+\varphi}-k_\varrho\sum_{i=1}^{6}\xi_i^{\bar{\varrho}}\\&-\Big(\frac{k_\sigma\delta_0}{2}\tilde{\boldsymbol{\sigma}}^T\tilde{\boldsymbol{\sigma}}\Big)^{\frac{1+\varphi}{2}}-\Big(\frac{k_\sigma\delta_0}{2}\tilde{\boldsymbol{\sigma}}^T\tilde{\boldsymbol{\sigma}}\Big)^{\frac{\bar{\varrho}}{2}}+\Phi\end{aligned}\tag{19}$$

where

$$\Phi=\begin{cases}\sigma_f+\frac{k_\sigma}{2}\boldsymbol{\sigma}^T\boldsymbol{\sigma}+\delta_0^{\frac{1+\varphi}{2}}\Phi_1, & \text{if } \Delta<\sqrt{2/(k_\sigma\delta_0)}\\ \sigma_f+\frac{k_\sigma}{2}\boldsymbol{\sigma}^T\boldsymbol{\sigma}+\delta_0^{\frac{1+\varphi}{2}}\Phi_1 & \text{if } \Delta\ge\sqrt{2/(k_\sigma\delta_0)}\\ +(\frac{k_\sigma\delta_0}{2}\Delta^2)^{\frac{\bar{\varrho}}{2}}-\frac{k_\sigma\delta_0}{2}\Delta^2,\end{cases}$$

Similar to (12)-(14), (18) finally becomes

$$\dot{V}_2\le-2^{-\frac{1+\varphi}{2}}k'_\varphi V_2^{\frac{1+\varphi}{2}}-2^{-\frac{\bar{\varrho}}{2}}13^{\frac{1-\varphi-\varrho}{2}}k'_\varrho V_2^{\frac{\bar{\varrho}}{2}}+\Phi\tag{20}$$

where $k'_\varphi=\min\{k_\varphi,(\frac{k_\sigma\delta_0}{2})^{\frac{1+\varphi}{2}}\}$ and $k'_\varrho=\min\{k_\varrho,(\frac{k_\sigma\delta_0}{2})^{\frac{\bar{\varrho}}{2}}\}$. Since (20) satisfies Lemma 2, the trajectory of (6) is therefore proven to be practical fixed-time stable. The residual set and setting time can be explicitly shown as in Lemma 2. □

Remark 1. From Assumption 3, the external disturbance is understood to be bounded by $\boldsymbol{\sigma}$. In addition, the configuration of the adaptive law (16) will ensure that $\hat{\boldsymbol{\sigma}}$ is bounded as well. Therefore, it is reasonable to adopt $\|\tilde{\boldsymbol{\sigma}}\|\le\Delta$ in the proof of Theorem 2.

Remark 2. As compared to the finite-time methods in [24–26], the controllers in our method specifically include the additional terms $\lceil\boldsymbol{k}_2\rfloor\boldsymbol{z}_1^{\varrho}$ and $\lceil\boldsymbol{k}_4\rfloor\boldsymbol{\xi}^{\varrho}$, which plays an integral role in solving the fixed-time tracking problem. When $\boldsymbol{k}_2=\boldsymbol{0}$ and $\boldsymbol{k}_4=\boldsymbol{0}$, the controllers in (7) and (15) can be simplified to take the form of finite-time regulation controllers. Moreover, if we set $\boldsymbol{k}_2=\boldsymbol{0}$, $\boldsymbol{k}_4=\boldsymbol{0}$ and $\varphi=1$ in (7), (15) and (16), then the traditional asymptotically tracking controllers are acquired. Comparative simulations based on these three controllers namely fixed-time, finite-time and traditional, are discussed in the following chapter.

Remark 3. Although the control design for a stratospheric airship being subjected to external disturbances is investigated, the proposed adaptive fixed-time control scheme can be easily extended to handle a more general class of second-order nonlinear system described by $\boldsymbol{M}\ddot{\boldsymbol{x}}=\boldsymbol{C}(\boldsymbol{x},\dot{\boldsymbol{x}})+\boldsymbol{\tau}+\boldsymbol{f}$, where $\boldsymbol{x}\in\mathbb{R}^n$ is the vector of system states, $\boldsymbol{M}\in\mathbb{R}^{n\times n}$ is the known matrix, $\boldsymbol{C}(\boldsymbol{x},\dot{\boldsymbol{x}})$ is a known nonlinear function, $\boldsymbol{\tau}\in\mathbb{R}^n$ is the control input, $\boldsymbol{f}\in\mathbb{R}^n$ is unknown external disturbance. This model is suitable in describing many practical systems like missiles [31], spacecrafts [37, 39], ships [40–43], and crane systems [44, 45].

Remark 4. Unlike the terminal sliding mode control methods in [27, 31–37] that can also achieve finite-time or fixed-time stability, the control signals of the proposed method are smooth without the presence of chattering. The method also does not require any signum operator. This is essential for the long-duration flight of the stratospheric airship, since the chattering of the control signals will reduce the lifetime of actuators. In addition, although we only achieve convergence towards a residual set in fixed-time, our approach is more realistic and moreover, the residual set can be set sufficiently small by tuning the control parameters.

Remark 5. The proposed fixed-time method are mainly inspired by [29, 30]. The main improvements are summarized as: 1) We extend the adding a power integrator method to the MIMO airship system. 2) The proposed adaptive method does not require the knowledge of disturbances and is computationally simple. 3) In [29, 30], the signum operator is introduced to eliminate the influence of uncertainties that results in control input chattering. Conversely, our proposed method eliminates the requirement of the signum operator that results in control signals which are smooth. 4) The controller parameters in [29, 30] must satisfy the limit of more than 1. We relaxed this limit to (8). Therefore, the control parameters can be arbitrarily chosen.

Remark 6. The proposed control scheme which is developed for the airship problem can also be easily extended to other second-order nonlinear systems and high-order MIMO nonlinear systems.

4. Simulations

A three-dimensional helix is selected as the desired trajectory of the simulation study to evaluate the performance of the proposed control method. The required coefficients and parameter values for the stratospheric airship are obtained from [12], that include $m = 5.6 \times 10^4(\text{kg})$, $\nabla = 7.4 \times 10^5(\text{m}^3)$, $\{x_g, z_g\} = \{5, 15\}(\text{m})$, $\{x_p, y_p, z_p\} = \{4, 0, 40\}(\text{m})$, $I_x = 5\times10^7(\text{kgm}^2)$, $I_y = 2.9\times10^8(\text{kgm}^2)$, $I_z = 2.9\times10^8(\text{kgm}^2)$, $I_{xz} = -6\times10^4(\text{kgm}^2)$, $\mu = \pi/6(\text{rad})$,$g = 9.81(\text{m/s}^2)$, $k_1' = 0.17$, $k_2' = 0.83$, $k_3' = 0.52$, $C_{l1} = 2.4\times10^4$, $C_{mi} = C_{ni} = 7.7\times10^4$, $C_{xi} = C_{yi} = C_{zi} = 657, i = 1, 2, 3, 4$. The air density ρ is determined by the flight altitude. The desired trajectory that resembles an ascending helical flight trajectory can be described as $\boldsymbol{\zeta}_c = [500\sin(0.01t), 500\cos(0.01t), -2t - 20000]^{\mathrm{T}}(\text{m})$. The airship is initially located at $\boldsymbol{\zeta}(0) = [100, 400, -19800]^{\mathrm{T}}(\text{m})$, while $\boldsymbol{\upsilon}(0) = [5, 0, 0]^{\mathrm{T}}(\text{m/s})$. The angular variables $\boldsymbol{\gamma}$ and $\boldsymbol{\omega}$ are initialized to zero. The time-varying external disturbances are given as $\boldsymbol{f} = 5000\times[0.5 + 2\sin(0.1t), 0.4 + 1.5\cos(0.1t), 0.6 + 1.5\sin(0.1t), 1.5 + 2\sin(0.1t), 1.5 + 1.5\sin(0.1t), 1.5 + 2\cos(0.1t)]^T$. The control parameters are chosen as $\varphi = 13/15$, $\varrho = 10/9$, $\boldsymbol{k}_1 = [0.05, 0.05, 0.05, 0.2, 0.2, 0.4]^T$, $\boldsymbol{k}_2 = [0.1, 0.1, 0.1, 0.1, 0.1, 0.2]^T$, $\boldsymbol{k}_3 = [1, 0.1, 1, 10^{-5}, 10^{-5}, 10^{-5}]^T$, $\boldsymbol{k}_4 = [10, 180, 10, 0.1, 0.1, 0.1]^T$, $k_\sigma = 10, \eta = 0.01$.

Based on the proposed adaptive fixed-time trajectory tracking controller, the results of the simulation study are presented in Figs. 2-5. The three-dimensional helical trajectory tracking is illustrated in Fig. 2, while the corresponding six-degrees-of-freedom position and velocity tracking errors are shown in Figs. 3-4. The control input profiles are plotted in Fig. 5. It can be observed in Figs. 2-4 that the tracking errors of the airship, being subjected to disturbances, converge to a small neighborhood of zero with a smooth transient response performance. As depicted in Fig. 5, the computed control inputs are continuous without exhibiting any chattering phenomenon. It is important to note that the initial control torques and forces are large in order to propel the airship to the desired trajectory swiftly. However, they do decrease rapidly once the desired position is achieved. These simulation results successfully demonstrate the remarkable response and control performance of the closed-loop system.

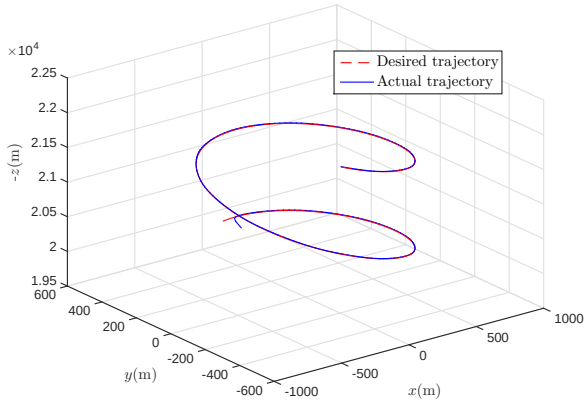

Figure 2: Trajectory for helix tracking.

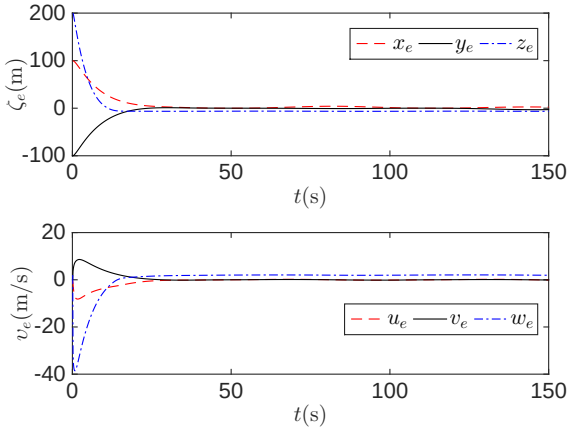

Figure 3: Position/velocity errors of fixed-time method.

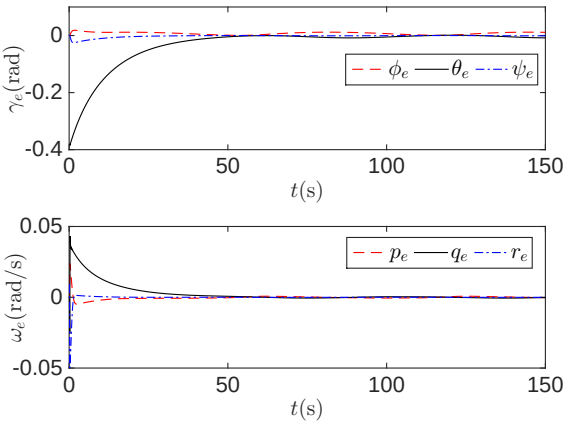

Figure 4: Attitude/angular velocity errors of fixed-time method.

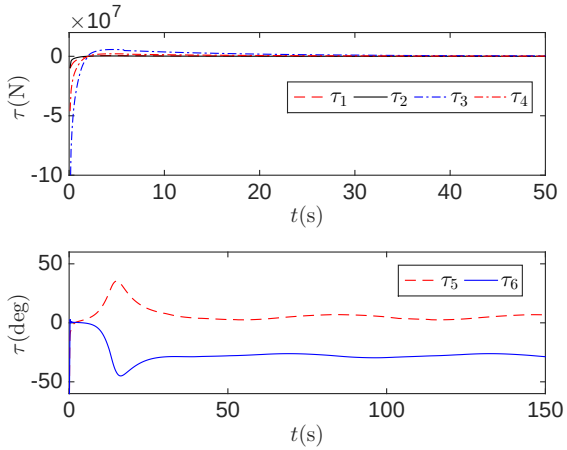

Figure 5: Inputs of fixed-time method.

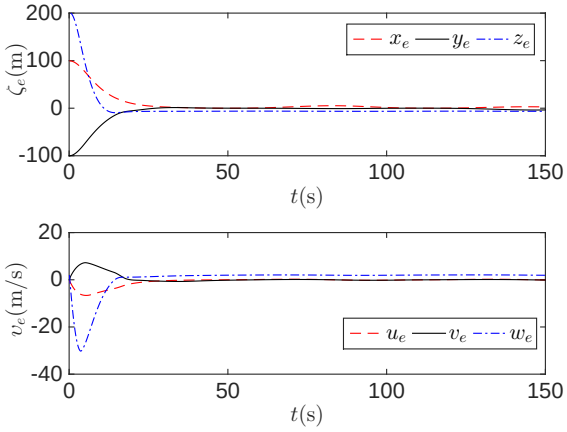

Figure 6: Position and velocity errors of finite-time method.

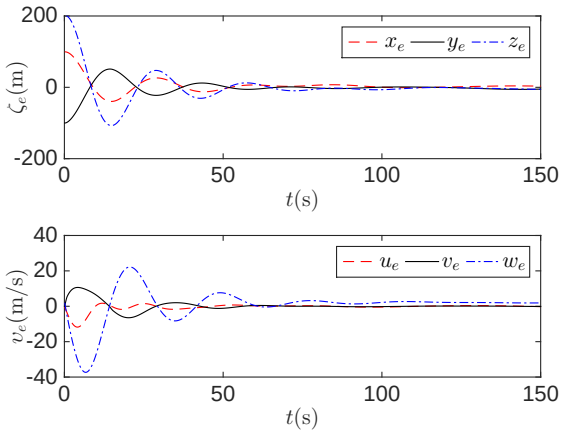

Figure 7: Position and velocity errors of method in [12].

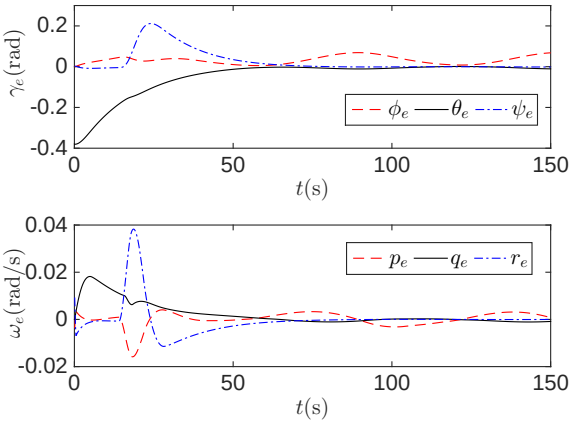

Figure 8: Attitude and angular velocity errors of finite-time method.

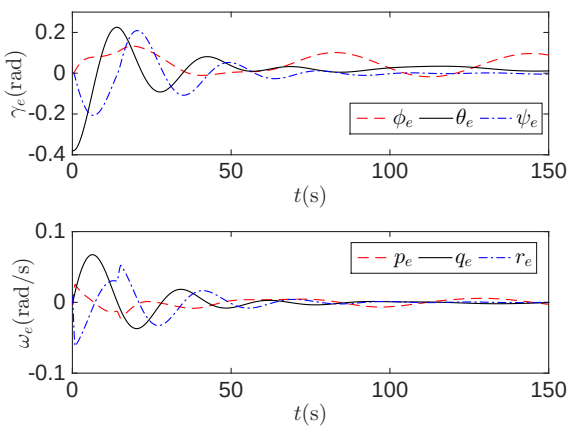

Figure 9: Attitude and angular velocity errors of method in [12].

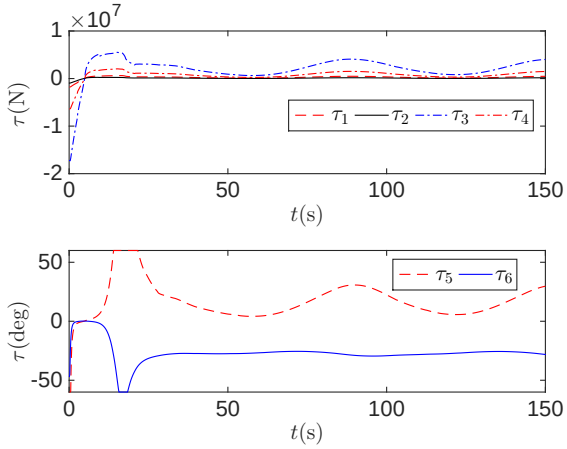

Figure 10: Inputs of finite-time method.

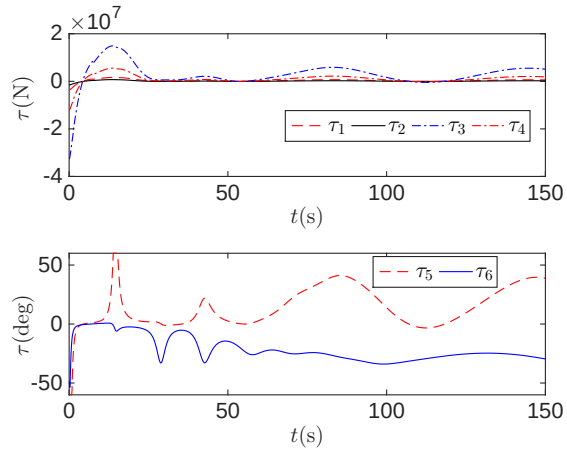

Figure 11: Inputs of method in [12].

Table 1: Performance Comparisons of Different Methods

	error	fixed-time	finite-time	method in [12]
IAE	$\boldsymbol{\zeta}_e$(m)	3464.0	4119.3	6194.9
	$\boldsymbol{\upsilon}_e$(m/s)	660.34	679.04	1192.8
	$\boldsymbol{\gamma}_e$(rad)	6.3371	16.289	20.972
	$\boldsymbol{\omega}_e$(rad/s)	0.5639	1.1660	3.1733
ITAE	$\boldsymbol{\zeta}_e$(m)	1.115×10^5	1.201×10^5	1.768×10^5
	$\boldsymbol{\upsilon}_e$(m/s)	2.600×10^4	2.724×10^4	4.050×10^4
	$\boldsymbol{\gamma}_e$(rad)	176.50	665.76	1020.7
	$\boldsymbol{\omega}_e$(rad/s)	12.613	45.998	105.33
ISE	$\boldsymbol{\tau}$(N)	0.489×10^{17}	1.772×10^{17}	3.608×10^{17}

Subsequently, to study the advantages of the proposed fixed-time controller, comparative simulations between different methods are carried out. The finite-time controller in Remark 2 and the traditional tracking controller in [12] are implemented to track the helical trajectory of the airship in the presence of disturbances. The control parameters in [12] are chosen as $k_p = 0.05, k_d = 0.1, k_z = 0.2$ and $\delta = 10$, which are consistent with the control parameters of our method.

The corresponding simulation results are shown in Figs. 6-11, where the position and velocity tracking errors are given in Figs. 6-7, the attitude and angular velocity tracking errors are presented in Figs. 8-9 and the control inputs are shown in Figs. 10-11. It can be observed that the transient response time is larger as compared to that of Figs. 3-4. In addition, the tracking errors of finite-time method suddenly become large at around 20 seconds in Fig. 8. This is because the calculated inputs of the finite time controller exceed the constraints of actuators, causing it to be saturated, which in turn deteriorates the control performance. To alleviate the effects of input saturation, some compensation methods [3, 46] can further be introduced. Moreover, to present the results more clearly and quantitatively, we summarize the performance comparisons of these methods based on the integrated absolute error, IAE (defined as $\int_0^t |e(\tau)|d\tau$), the integrated time absolute error, ITAE (defined as $\int_0^t t|e(\tau)|d\tau$) and the integral of square error, ISE (defined as $\int_0^t u(\tau)^2 d\tau$) in Table 1. The IAE, ITAE and ISE metrics are introduced to evaluate the transient performance, the steady-state performance and the control energy of trajectory tracking controller respectively [26, 47]. As observed in Table 1, it is evident that the proposed fixed-time method provides a better dynamic performance as compared to other methods as it leads to the lowest IAE and ITAE values with the smallest control energy consumption ISE.

It is observed from Lemma 2 that the residual set and the setting time T are partly determined by control gains. To demonstrate the effect of parameter variations, we reduced the control gains to 30% of $\boldsymbol{k}_i, i = 1, \cdots, 4$. The results of trajectory tracking errors and inputs with these smaller control gains are shown in Figs. 12-13. It is evident that larger control gains lead to smaller residual set and setting time, however at the expense of bigger inputs. As such, a compromise between control performance and actuator constraint should be made in practical problems. Moreover, to test the performance of the proposed method under noise, we increase the external disturbance to $\boldsymbol{f} = 20000\times\texttt{rand(0,1)}\times[0.5+2\sin(0.1t), 0.4+1.5\cos(0.1t), 0.6+1.5\sin(0.1t), 1.5+5\sin(0.1t), 1.5+5\sin(0.1t), 1.5+5\cos(0.1t)]^T$, where `rand(0,1)` means the random number in $(0, 1)$. The results of trajectory tracking errors and inputs with noise are given in Figs. 14-15. We can observe that even if there exists noise and large disturbances, the proposed method is still able to work properly and maintain acceptable tracking performance. In addition, to test the performance of the proposed method under varying initial states, a different initial position, given by $\boldsymbol{\zeta}(0) = [-300, 600, -20500]^{\mathrm{T}}$(m), is specified for the airship. The results of trajectory tracking errors are given in Fig. 16, which demonstrates that the controller is still valid under different initial conditions.

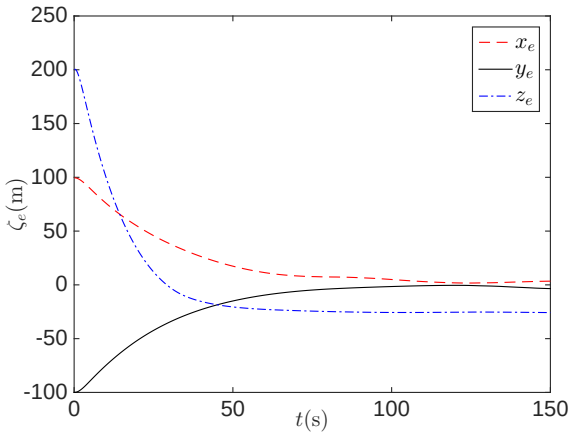

Figure 12: Trajectory of fixed-time method with smaller control gains.

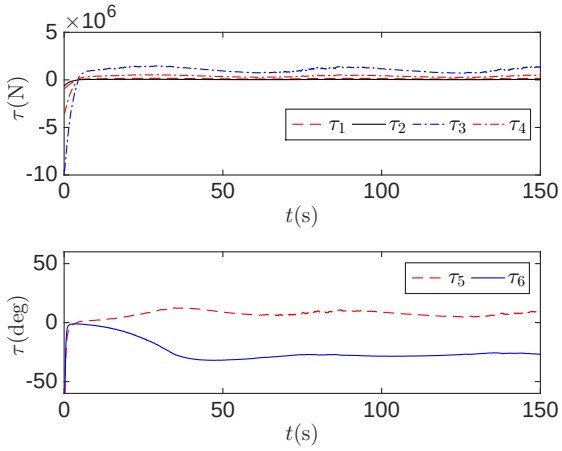

Figure 13: Inputs of fixed-time method with smaller control gains.

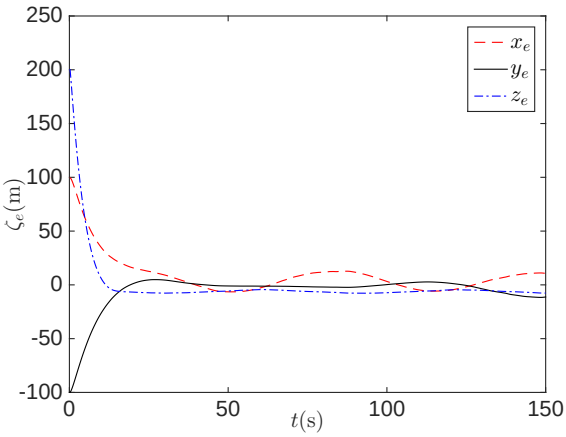

Figure 14: Trajectory of fixed-time method with noise.

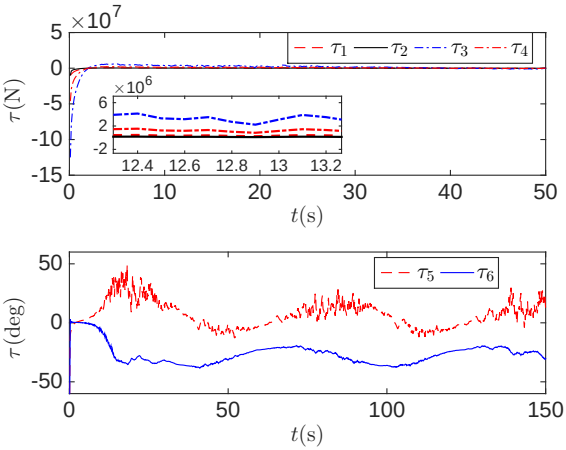

Figure 15: Inputs of fixed-time method with noise.

5. Conclusion

Driven by the practical requirements of faster and quantifiable convergence for the stratospheric airship, an adaptive fixed-time based trajectory tracking control algorithm is presented for the airship's motion control while being subjected to external disturbances. The method of adding a power integrator technique, which is subsequently integrated into the Lyapunov synthesis, successfully ensures that the tracking errors of the stratospheric airship converge towards a residual set within fixed-time. Comprehensive simulations of the proposed control method compared with other methods have illustrated the enhanced performance of the proposed controller. The proposed trajectory tracking control method can be easily utilized to other nonlinear systems, although it is designed specifically for airship. In future work, this method may be extended to unmanned vehicles under actuator saturation and faults.

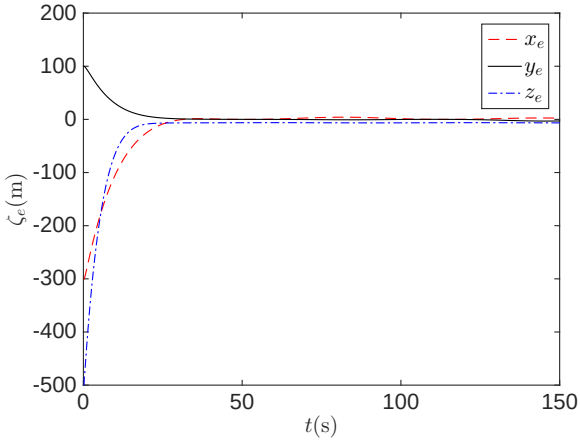

Figure 16: Trajectory of fixed-time method with different initial states.

Acknowledgments

This work was supported in part by the National Natural Science Foundation of China under Grant 61503010 and 61703018, in part by the Aeronautical Science Foundation of China under Grant 2016ZA51001, and in part by the Fundamental Research Funds for the Central Universities under Grant YWF-17-BJ-Y-143.

References

[1] Isaac Vandermeulen, Martin Guay, and P James McLellan. Distributed control of high-altitude balloon formation by extremum-seeking control. *IEEE Transactions on Control Systems Technology*, 2017, advance online publication.

[2] Zewei Zheng and Liang Sun. Error-constrained path-following control for a stratospheric airship with actuator saturation and disturbances. *International Journal of Systems Science*, 48(16):3504–3521, 2017.

[3] Zewei Zheng and Lihua Xie. Finite-time path following control for a stratospheric airship with input saturation and error constraint. *International Journal of Control*, 2017, advance online publication.

[4] Lihua Liu, Zongyang Shi, Kai Wu, Zhi Geng, and Guangyou Fang. A bipolar half-sine current inverter for airship-borne electromagnetic (aem) surveying. *IEEE Transactions on Industrial Electronics*, 64(12):9477–9486, 2017.

[5] Xixiang Yang. Prediction of thermal behavior and trajectory of stratospheric airships during ascent based on simulation. *Advances in Space Research*, 57(11):2326–2336, 2016.

[6] Zewei Zheng and Liang Sun. Adaptive sliding mode trajectory tracking control of robotic airships with parametric uncertainty and wind disturbance. *Journal of the Franklin Institute*, 355(1):106–122, 2018.

[7] Zhouhua Peng, Jun Wang, and Dan Wang. Distributed containment maneuvering of multiple marine vessels via neurodynamics-based output feedback. *IEEE Transactions on Industrial Electronics*, 64(5):3831–3839, 2017.

[8] Emre Sariyildiz, Gong Chen, and Haoyong Yu. Robust trajectory tracking control of multimass resonant systems in state space. *IEEE Transactions on Industrial Electronics*, 64(12):9366–9377, 2017.

[9] Khac Duc Do. Synchronization motion tracking control of multiple underactuated ships with collision avoidance. *IEEE Transactions on Industrial Electronics*, 63(5):2976–2989, 2016.

[10] Zewei Zheng, Cheng Jin, Ming Zhu, and Kangwen Sun. Trajectory tracking control for a marine surface vessel with asymmetric saturation actuators. *Robotics and Autonomous Systems*, 97:83–91, 2017.

[11] Erlin Zhu, Jinfeng Pang, Na Sun, Haitao Gao, Qinglin Sun, and Zengqiang Chen. Airship horizontal trajectory tracking control based on active disturbance rejection control (adrc). *Nonlinear Dynamics*, 75(4):725–734, 2014.

[12] Liang Sun and Zewei Zheng. Nonlinear adaptive trajectory tracking control for a stratospheric airship with parametric uncertainty. *Nonlinear Dynamics*, 3(82):1419–1430, 2015.

[13] Yueneng Yang and Ye Yan. Neural network approximation-based nonsingular terminal sliding mode control for trajectory tracking of robotic airships. *Aerospace Science and Technology*, 54:192–197, 2016.

[14] Lotfi Beji and Azgal Abichou. Tracking control of trim trajectories of a blimp for ascent and descent flight manoeuvres. *International Journal of Control*, 78(10):706–719, 2005.

[15] Zewei Zheng, Wei Huo, and Zhe Wu. Trajectory tracking control for underactuated stratospheric airship. *Advances in Space Research*, 50(7):906–917, 2012.

[16] Alexandra Moutinho, José Raul Azinheira, Ely C de Paiva, and Samuel S Bueno. Airship robust path-tracking: A tutorial on airship modelling and gain-scheduling control design. *Control Engineering Practice*, 50:22–36, 2016.

[17] Ricardo C. Do Valle, Luciano L. Menegaldo, and Alberto M. Simoes. Smoothly gain-scheduled control of a tri-turbofan airship. *Journal of Guidance Control & Dynamics*, 38(1):53–61, 2015.

[18] David K Schmidt. Modeling and near-space stationkeeping control of a large high-altitude airship. *Journal of Guidance Control and Dynamics*, 30(2):540, 2007.

[19] Zewei Zheng and Yao Zou. Adaptive integral los path following for an unmanned airship with uncertainties based on robust rbfnn backstepping. *ISA transactions*, 65:210–219, 2016.

[20] Zewei Zheng and Wei Huo. Planar path following control for stratospheric airship. *IET Control Theory & Applications*, 7(2):185–201, 2013.

[21] Zewei Zheng, Wei Huo, and Zhe Wu. Autonomous airship path following control: Theory and experiments. *Control Engineering Practice*, 21(6):769–788, 2013.

[22] L Chen, DP Duan, and DS Sun. Design of a multi-vectored thrust aerostat with a reconfigurable control system. *Aerospace Science and Technology*, 53:95–102, 2016.

[23] Torsten Liesk, Meyer Nahon, and Benoit Boulet. Design and experimental validation of a nonlinear low-level controller for an unmanned fin-less airship. *IEEE Transactions on Control Systems Technology*, 21(1):149–161, 2013.

[24] Zong-Yao Sun, Xing-Hui Zhang, and Xue-Jun Xie. Continuous global stabilisation of high-order time-delay nonlinear systems. *International Journal of Control*, 86(6):994–1007, 2013.

[25] Shihua Li, Haibin Sun, Jun Yang, and Xinghuo Yu. Continuous finite-time output regulation for disturbed systems under mismatching condition. *IEEE Transactions on Automatic Control*, 60(1):277–282, 2015.

[26] Ning Wang, Chunjiang Qian, Jing-Chao Sun, and Yan-Cheng Liu. Adaptive robust finite-time trajectory tracking control of fully actuated marine surface vehicles. *IEEE Transactions on Control Systems Technology*, 24(4):1454–1462, 2016.

[27] Andrey Polyakov. Nonlinear feedback design for fixed-time stabilization of linear control systems. *IEEE Transactions on Automatic Control*, 57(8):2106–2110, 2012.

[28] Zhongcai Zhang and Yuqiang Wu. Fixed-time regulation control of uncertain nonholonomic systems and its applications. *International Journal of Control*, 90(7):1327–1344, 2017.

[29] Jinming Huang and Zhongcai Zhang. Nonlinear feedback design for fixed-time tracking of a class of nonlinear systems. *International Journal of Computer Mathematics*, 94(7):1349–1362, 2017.

[30] Yana Yang, Changchun Hua, Junpeng Li, and Xinping Guan. Robust adaptive uniform exact tracking control for uncertain euler–lagrange system. *International Journal of Control*, 90(12):2711–2720, 2017.

[31] Michael V Basin, Polk Yu, and Yuri B Shtessel. Hypersonic missile adaptive sliding mode control using finite-and fixed-time observers. *IEEE Transactions on Industrial Electronics*, 65(1):930–941, 2018.

[32] Zongyu Zuo. Nonsingular fixed-time consensus tracking for second-order multi-agent networks. *Automatica*, 54:305–309, 2015.

[33] Junkang Ni, Ling Liu, Chongxin Liu, and Jian Liu. Fixed-time leader-following consensus for second-order multiagent systems with input delay. *IEEE Transactions on Industrial Electronics*, 64(11):8635–8646, 2017.

[34] Zongyu Zuo, Bailing Tian, Michael Defoort, and Zhengtao Ding. Fixed-time consensus tracking for multiagent systems with high-order integrator dynamics. *IEEE Transactions on Automatic Control*, 63(2):563–570, 2018.

[35] Bailing Tian, Zongyu Zuo, Xiaomo Yan, and Hong Wang. A fixed-time output feedback control scheme for double integrator systems. *Automatica*, 80:17–24, 2017.

[36] Boyan Jiang, Qinglei Hu, and Michael I Friswell. Fixed-time rendezvous control of spacecraft with a tumbling target under loss of actuator effectiveness. *IEEE Transactions on Aerospace and Electronic Systems*, 52(4):1576–1586, 2016.

[37] Boyan Jiang, Qinglei Hu, and Michael I Friswell. Fixed-time attitude control for rigid spacecraft with actuator saturation and faults. *IEEE Transactions on Control Systems Technology*, 24(5):1892–1898, 2016.

[38] Zewei Zheng, Yanting Huang, Lihua Xie, and Bing Zhu. Adaptive trajectory tracking control of a fully actuated surface vessel with asymmetrically constrained input and output. *IEEE Transactions on Control Systems Technology*, 2017, advance online publication.

[39] Liang Sun and Zewei Zheng. Disturbance-observer-based robust backstepping attitude stabilization of spacecraft under input saturation and measurement uncertainty. *IEEE Transactions on Industrial Electronics*, 64(10):7994–8002, 2017.

[40] Zewei Zheng and Mir Feroskhan. Path following of a surface vessel with prescribed performance in the presence of input saturation and external disturbances. *IEEE/ASME Transactions on Mechatronics*, 22(6):2564–

2575, 2017.

[41] Zewei Zheng, Liang Sun, and Lihua Xie. Error-constrained los path following of a surface vessel with actuator saturation and faults. *IEEE Transactions on Systems Man & Cybernetics Systems*, 2017, advance online publication.

[42] Xianbo Xiang, Chao Liu, Housheng Su, and Qin Zhang. On decentralized adaptive full-order sliding mode control of multiple uavs. *ISA transactions*, 71:196–205, 2017.

[43] Wenjing Xie, Baoli Ma, Tyrone Fernando, and Herbert Ho-Ching Iu. A simple robust control for global asymptotic position stabilization of underactuated surface vessels. *International Journal of Robust and Nonlinear Control*, 27(18):5028–5043, 2017.

[44] Ning Sun, Yiming Wu, Yongchun Fang, and He Chen. Nonlinear antiswing control for crane systems with double-pendulum swing effects and uncertain parameters: Design and experiments. *IEEE Transactions on Automation Science and Engineering*, 2017, advance online publication.

[45] Ning Sun, Yongchun Fang, He Chen, Yiming Fu, and Biao Lu. Nonlinear stabilizing control for ship-mounted cranes with ship roll and heave movements: Design, analysis, and experiments. *IEEE Transactions on Systems, Man, and Cybernetics: Systems*, 2017, advance online publication.

[46] Ning Sun, Yongchun Fang, He Chen, and Biao Lu. Amplitude-saturated nonlinear output feedback antiswing control for underactuated cranes with double-pendulum cargo dynamics. *IEEE Transactions on Industrial Electronics*, 64(3):2135–2146, 2017.

[47] Samir Zeghlache, Tarak Benslimane, and Abderrahmen Bouguerra. Active fault tolerant control based on interval type-2 fuzzy sliding mode controller and non linear adaptive observer for 3-dof laboratory helicopter. *ISA transactions*, 71:280–303, 2017.